Analysis of Pion-Helium Scattering for the Pion Charge Form Factor*

C. T. Mottershead†
Lawrence Radiation Laboratory, University of California, Berkeley, California 94720
(Received 14 August 1969; revised manuscript received 23 February 1972)

Elastic scattering of π^+ and π^- on He^4 is analyzed for information on the charge radius of the pion using a new method based on boundary conditions near the nuclear surface. The pion radius enters the calculation via the electrostatic potential of the pion and helium charge distributions, which is assumed to be the only charge-dependent interaction. Since He^4 is isoscalar, the strong nuclear interaction is assumed to be charge-independent. Differential cross-section data for both signs of the charge are fitted simultaneously by a program that uses the logarithmic derivatives of the pion radial wave function for each charge as free parameters. If the nuclear interaction operator is symmetric (i.e., $\langle\vec{r}'|U_N|\vec{r}\rangle = \langle\vec{r}|U_N|\vec{r}'\rangle$), the difference in the logarithmic derivative for a given partial wave resulting from changing the sign of the charge may be expressed as an integral of the internal Coulomb potential weighted by the wave function. Nuclear model dependence is greatly reduced by the constraints imposed by the empirical boundary conditions on the internal wave function. The Berkeley data at beam momenta of 130 to 163 MeV/c are analyzed by this method using both local potential and Kisslinger models for the strong interaction, and Gaussian and Yukawa pion charge distributions. The results indicate $2.2 < r_\pi < 3.2$ F, depending on the theoretical model, with an experimental precision of $\sim \pm 0.5$ F. In the course of the analysis, the singular-point difficulty with the Kisslinger model was examined and found to be serious.

I. INTRODUCTION

The possibility of measuring the pion electromagnetic form factor by comparing the elastic scattering of π^+ and π^- beams on an isoscalar target nucleus such as He^4 has been the subject of a series of recent papers.[1-14] The key assumption of these studies is that the strong nuclear interaction, whatever its detailed nature, is the same for both pion charges, while the Coulomb potential is the same except for sign. This Coulomb potential, which is taken to be the only electromagnetic interaction, depends on the charge distributions of the pion and nucleus, and thus on the parameters of their respective form factors. The general plan is to analyze the differential cross-section data for both charges to separate the nuclear and Coulomb contributions to the scattering amplitude. If the nuclear charge distribution is known, the Coulomb contribution may then be interpreted as a measurement of the pion charge radius.

Accurate calculations, with the fewest possible approximations, are needed to find the small effects due to pion size in the large nuclear scattering amplitudes. It is also essential to reduce the effect of the uncertainties in the pion-nucleus interaction by using model-independent methods as far as possible. With these objectives, two methods of analysis have so far been proposed:

(i) Optical-model analysis. The emphasis here is on calculational accuracy.[1-4] The nuclear interaction is represented by an optical-model potential and the Schrödinger equation integrated numerically for both signs of the charge. The parameters of both the optical and Coulomb potentials are then adjusted to fit the cross-section data. An exact solution is obtained for the given model, but the method mixes the Coulomb and nuclear parts of the problem, so the pion radius obtained may depend on the model chosen.

(ii) Coulomb perturbation methods. These emphasize model independence.[5-13] The nuclear amplitude is parametrized by a set of phase shifts, and the Coulomb–Born amplitude, which is proportional to the product of the form factors, is explicitly separated out. The method is less model-dependent than (i), and it avoids the use of Coulomb wave functions, but it introduces an important first-order Coulomb-nuclear interference ("distortion") amplitude that is given by a logarithmically divergent integral.

A third method of analysis, using the same basic assumptions as the above two, is proposed in Sec. II of this paper in an effort to combine calculational accuracy with model independence. A close-fitting boundary surface (radius R) is drawn around the nucleus, and the Coulomb potential $\pm Ze^2/r$ is assumed to be the only interaction in the external region ($r \geq R$). As in (i), the exact external solution of the Schrödinger equation is expressed in terms of Coulomb wave functions, and related to the logarithmic derivative of the interior solution at the boundary. These logarithmic derivatives, however, are taken as free parameters, thus giving a model-independent fit to the cross-section data, while avoiding the divergence difficulties

that arise in perturbation treatments of the long-range part of the Coulomb potential. The interior Coulomb perturbation on the logarithmic derivatives is then derived for a very general form of nuclear interaction operator, and turns out to be only slightly model-dependent.

In Sec. III the method is applied to the Berkeley data[3] to determine the empirical boundary conditions at $r=R$. The relevant aspects of models for the pion-nucleus interaction are discussed in Sec. IV, and the conclusions about the pion size given in Sec. V. Finally, the effects of some alternative assumptions are discussed in Sec. VI.

II. THE BOUNDARY CONDITION METHOD

The Klein-Gordon equation for the motion of a pion of energy E_π and charge te ($t=+1$, 0, or -1) in a fixed electrostatic potential Ze/r may be written

$$[\nabla^2 + k^2 - t\,2\eta k/r]\Psi^t(\vec{\mathbf{r}}) = 0\,, \tag{1}$$

where $k=(E_\pi{}^2 - m_\pi{}^2)^{1/2}$ is the asymptotic momentum of the pion, and $\eta = Ze^2/\beta$ is the Coulomb scattering strength parameter for velocity $\beta = k/E_\pi$. A second-order term in the potential, which is less than $10^{-4}k^2$ for our pion-helium scattering problem, has been omitted from Eq. (1) so that conventional Coulomb functions may be used in its solution. We slightly generalize Eq. (1) by taking k to be the momentum and β the relative velocity in the center-of-mass coordinate system as computed according to conventional two-body relativistic kinematics. Then $\Psi^t(\vec{\mathbf{r}})$ is interpreted as the probability amplitude for the interparticle separation $\vec{\mathbf{r}}$. This compromise to allow for both nuclear recoil motion and relativistic kinematics leads to $k\eta = Z\alpha E$, where $E \equiv E_\pi E_N/(E_\pi + E_N)$ is the "reduced energy" in terms of the center-of-mass energies of the pion and nucleus. The numerical values of k, η and the kinetic energies $T_\pi = E_\pi - m_\pi$ and $T_\alpha = E_N - M_\alpha$ (with $m_\pi = 139.6$ MeV and $M_\alpha = 3727.6$ MeV) are listed in Table I. In any case, we assume Eq. (1) applies to the pion-nucleus system when the pion is outside some small sphere of radius R centered on the nucleus.

Substitution of a partial-wave expansion into Eq. (1) results in a set of Coulomb radial equations which have the general solutions (for $l=0, 1, 2, \ldots$ and $r \geq R$)

$$u_l^t(r) = A_l^t[\cos\delta_l^t F_l(t\eta, kr) + \sin\delta_l^t G_l(t\eta, kr)]\,, \tag{2}$$

where $F_l(\eta, x)$ and $G_l(\eta, x)$ are the standard regular and irregular Coulomb functions, A_l^t are normalization constants, and δ_l^t are the "nuclear phase shifts" due to whatever deviations there are (for $r<R$) from a pure $1/r$ potential. The corresponding differential cross section for elastic scattering may be written

$$\sigma^t(\theta) = |f_N^t(\theta) + f_C^t(\theta)|^2\,, \tag{3}$$

where, except for an unobservable phase, f_C^t is the usual pure Coulomb scattering amplitude

$$f_C^t(q) \equiv -\frac{2t\eta k}{q^2}\exp\left[-it\eta\ln\left(\frac{q^2}{4k^2}\right)\right], \tag{4}$$

and f_N^t is the nuclear scattering amplitude given by the partial-wave expansion

$$f_N^t(\theta) = \sum_{l=0}^{\infty}(2l+1)\gamma_l(t\eta)a_l^t(k)P_l(\cos\theta)\,. \tag{5}$$

Here θ is the center-of-mass scattering angle, $q^2 = 2k^2(1-\cos\theta)$ is the momentum transfer squared, and the partial-wave amplitude a_l^t is given by $a_l^t(k) \equiv (k\cot\delta_l^t - ik)^{-1}$. The Coulomb phase shifts $\sigma_l = \arg\Gamma(l+1+i\eta)$ are absorbed in the factors

$$\gamma_l(\eta) \equiv \exp 2i[\sigma_l(\eta) - \sigma_0(\eta)]\,, \tag{6}$$

which may be conveniently generated from the recursion formulas

$$\gamma_0(\eta) = 1\,,$$
$$\gamma_l(\eta) = \frac{(l+i\eta)^2}{(l^2+\eta^2)}\gamma_{l-1}(\eta)\,, \tag{7}$$
$$\gamma_l(-\eta) = \gamma_l^*(\eta)\,.$$

If Eq. (1) were valid for all r, then only the regular solution $F_l(\eta, x)$ would be permitted in Eq. (2), and all the δ_l^t would have to be zero. Equation (3) would then reduce to the well-known Rutherford formula for pure Coulomb scattering.

Of course Eq. (1) is not valid for all r. At small distances the electrostatic potential will deviate

TABLE I. Kinematics and fit quality.

Data set	p_{lab} (MeV/c)	k (F^{-1})	η	c.m. kinetic energy (MeV) T_π	T_α	i rms error $\bar{p}$	$\sigma_\pm(\theta)$ fits 30 data points χ_+^2	χ_-^2	χ_σ^2	$\Delta(\theta)$ fits 15 data points $\overline{\delta\Delta}$	χ_Δ^2
a	130.2	0.6280	0.0209	47.1	2.1	0.045	21.1	16.3	37.4	0.063	14.9
b	142.3	0.6850	0.0199	54.7	2.4	0.022	71.1	40.5	111.6	0.022	29.2
c	153.2	0.7361	0.0192	61.8	2.8	0.042	37.2	17.4	54.6	0.054	21.9
d	163.0	0.7818	0.0186	68.4	3.2	0.028	55.2	35.2	90.4	0.033	28.0

from the $1/r$ form due to overlap of the charge distributions of the pion and nucleus. The pion's charge form factor is related to its charge distribution $te\rho_\pi(r)$ by

$$F_\pi(q) = \int d^3r\, e^{-i\vec{q}\cdot\vec{r}}\rho_\pi(r), \tag{8}$$

where $\rho_\pi(r)$ is normalized so that

$$F_\pi(0) = \int d^3r\,\rho_\pi(r) = 1.$$

Expansion of Eq. (8) in powers of q yields

$$F(q) = 1 - \frac{1}{3!}q^2\langle r^2\rangle + \frac{1}{5!}q^4\langle r^4\rangle - \frac{1}{7!}q^6\langle r^6\rangle - \cdots, \tag{9a}$$

where

$$\langle r^n\rangle \equiv \int r^n\rho(r)4\pi r^2 dr \tag{9b}$$

is the nth moment of the charge distribution. Our objective is to measure the rms pion charge radius $r_\pi \equiv \langle r^2\rangle^{1/2}$ via its influence on the short-range behavior of the electrostatic potential between the pion and nucleus. This is given in terms of their form factors and the separation r of their centers by $V_C(r) \equiv tZe^2v(r)$ with

$$v(r) = \frac{1}{(2\pi)^3}\int d^3q\, e^{i\vec{q}\cdot\vec{r}}F_\pi(\vec{q})\frac{4\pi}{q^2}F_N(-\vec{q}). \tag{10}$$

For the nuclear form factor, we take the Gaussian[15]

$$F_N(q) = \exp(-q^2r_N^2/6) \tag{11a}$$

with the rms radius $r_N = 1.65 \pm 0.03$ F indicated by electron scattering on He^4. This corresponds to a Gaussian charge density

$$\rho_N(r) = \pi^{-3/2}a_N^{-3}\exp(-r^2/a_N^2) \tag{11b}$$

with width parameter $a_N = (\frac{2}{3})^{1/2}r_N$. For the pion form factor, we need to adopt a specific model whose parameters we can relate to r_π and $v(r)$. The simplest choice is to take the pion shape as also Gaussian: $F_\pi(q) = \exp(-q^2r_\pi^2/6)$. Then the effective charge distribution defined by

$$\rho_{\text{eff}}(r) \equiv (4\pi)^{-1}\nabla^2 v(r) \tag{12}$$

is again Gaussian with width parameter $c^2 = \frac{2}{3}(r_N^2 + r_\pi^2)$, and Eq. (12) may be readily integrated to give[16]

$$v_G(r) = \frac{1}{r}\,\text{erf}\left(\frac{r}{c}\right). \tag{13}$$

As a possibly more realistic alternative, and to check our sensitivity to the detailed shape of the pion form factor, we also use the simple one-pole model

$$F_\pi(q) = (1 + q^2/\mu^2)^{-1}, \tag{14a}$$

which leads to a Yukawa charge distribution

$$\rho_\pi(r) = \mu^2 e^{-\mu r}/4\pi r \tag{14b}$$

with $r_\pi = \sqrt{6}/\mu$. The corresponding potential is[17]

$$v_Y(r) = \frac{1}{r}\left\{\text{erf}\left(\frac{r}{a}\right) + \frac{1}{2}e^{(\mu a/2)^2}\left[e^{\mu r}\,\text{erfc}\left(\frac{\mu a}{2} + \frac{r}{a}\right) - e^{-\mu r}\,\text{erfc}\left(\frac{\mu a}{2} - \frac{r}{a}\right)\right]\right\}. \tag{15}$$

According to the vector-dominance model,[18] where μ is taken as the mass of the ρ meson, Eq. (14) is a good approximation to $F_\pi(q)$, at least near the pole at $q^2 = -\mu^2 = -15.1$ F^{-2}. The corresponding predicted pion radius is $r_\pi = 0.63$ F. The data of interest here, however, are for $0 \le q^2 \le 2.4$ F^{-2}, and we analyze it treating the r_π in Eqs. (13) and (15) as the unknown to be determined. For $r_\pi = 0$, Eqs. (13) and (15) give identical results. Figure 1 shows the He^4 density distribution, and the effective Coulomb potentials $V_c(r) = Ze^2v_G(r)$ calculated from Eq. (13) for $r_\pi = 0$, 1, 2, and 3 F. The po-

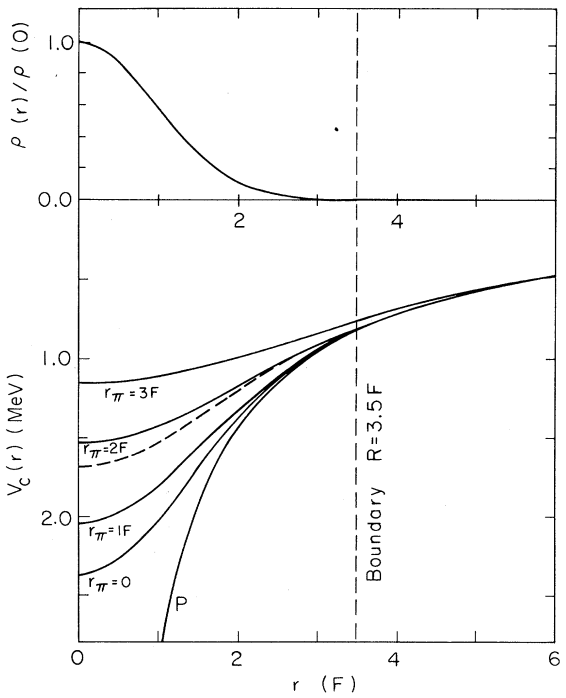

FIG. 1. Nuclear density distribution $\rho(r)/\rho(0)$, and effective Coulomb potentials $V_C(r)$ (MeV) for Gaussian pion charge distribution [Eq. (13)] with $r_\pi = 0$, 1, 2, and 3 F; Yukawa pion charge distribution [Eq. (15)] with $r_\pi = 2$ F (dashed curve); and pure $1/r$ potential of two point charges (curve P).

tential for $r_\pi = 2$ F according to Eq. (15), and for a point charge ($v_c = Ze^2/r$) are also shown for comparison. Beyond $R = 3.5$ F, which we choose as the boundary radius, we have essentially $\rho_N(r) = 0$ and $v(r) = 1/r$.

In addition to this Coulomb potential, the pion for $r < R$ feels a strong nuclear interaction which we will assume to be short-ranged, rotationally invariant, and charge-independent. We therefore generalize Eq. (1) in the form

$$\{\nabla^2 + k^2 - 2t\eta k v(r)\}\Psi^t(\vec{r}) = \int d^3r' \langle \vec{r}\,|U_N|\,\vec{r}'\rangle \Psi^t(\vec{r}'), \tag{16}$$

where $\langle \vec{r}\,|U_N|\,\vec{r}'\rangle$ is the coordinate representation of some nuclear interaction operator U_N. Charge independence means that U_N is the same for all values of the charge index t. We choose the boundary radius R so that in the external region $r \geq R$, U_N is negligible ($\langle \vec{r}\,|U_N|\,r'\rangle \cong 0$), and $v(r)$ takes its asymptotic form $1/r$, so Eq. (16) takes the form Eq. (1).

The assumption of rotational invariance means we can solve Eq. (16) one partial wave at a time. In a solution of the form

$$\Psi^t(\vec{r}) = \chi_l^t(r) Y_l^m(\theta, \Psi), \tag{17}$$

the radial wave function χ_l is determined to within a normalization constant by Eq. (16), and so its logarithmic derivative at the boundary $r = R$, defined by

$$\lambda_l^t \equiv R\left\{\frac{\partial}{\partial r} \ln(r\chi_l^t(r))\right\}_{r=R}, \tag{18}$$

is completely determined.

For the experiment in question (130–160 MeV/c $\pi^\pm$ on He[4]), the whole Coulomb potential $V_C(r)$ inside $r = R$ is a small perturbation on the energy and strong-interaction terms in Eq. (16). Therefore changing the sign of V_C should induce only a small shift in λ_l^t. Writing

$$\lambda_l^\pm(k, R) \equiv S_l(k, R) \pm \eta D_l(k, R), \tag{19}$$

we expect the average logarithmic derivative $S_l = \frac{1}{2}(\lambda_l^+ + \lambda_l^-)$ to depend mainly on the strong interaction, while the difference $D_l = (\lambda_l^+ - \lambda_l^-)/2\eta$ should depend mainly on the Coulomb effects. The nuclear phase shift δ_l^t corresponding to a given value of λ_l^t is obtained by substituting $r\chi_l^t(r) = u_l^t(r)$ into Eq. (18), where u_l^t is defined by Eq. (2). The parametrization of the observable nuclear partial-wave amplitudes by the variables S_l and D_l is then given by

$$a_l^\pm = -\frac{1}{k}\left\{\frac{(S_l \pm \eta D_l)F_l(\pm\eta, x) - xF_l'(\pm\eta, x)}{(S_l \pm \eta D_l)H_l(\pm\eta, x) - xH_l'(\pm\eta, x)}\right\}_{x=kR}, \tag{20}$$

where

$$H_l(\eta, x) \equiv G_l(\eta, x) + iF_l(\eta, x),$$

$$F_l'(\eta, x) \equiv \frac{\partial F_l(\eta, x)}{\partial x} \cdots, \quad \text{etc.}$$

A least-squares program, the details of which will be discussed in Sec. III, was used to adjust S_l and D_l for the first few partial waves to fit the Berkeley scattering data.[3] The use of S_l and D_l as free variables assures a fit as model-independent and general as phase-shift analysis, while combining data for both signs of the charge in an advantageous manner. The partial waves with $l \geq 3$ were found to be negligible, so the empirical values of S_l and D_l for $l \leq 2$ must contain all the information available in the experiment about both the nuclear interaction and the pion form factor.

To extract this information, we relate these quantities to the generalized interior model represented by Eq. (16) as follows: Multiply Eq. (16) by the wave function for charge index t', subtract the corresponding equation with t and t' interchanged, and integrate over the internal volume $|\vec{r}| \leq R$ to obtain

$$\int_{|\vec{r}|\leq R} d^3r \{\Psi^{t'}(r)\nabla^2\Psi^t(r) - \Psi^t(r)\nabla^2\Psi^{t'}(r) + 2\eta k(t' - t)v(r)\Psi^{t'}(r)\Psi^t(r)\}$$

$$= \int_{|\vec{r}|\leq R} d^3r \int d^3r' \{\Psi^{t'}(\vec{r})\langle \vec{r}\,|U_N|\,\vec{r}'\rangle \Psi^t(\vec{r}') - \Psi^t(\vec{r})\langle \vec{r}\,|U_N|\,\vec{r}'\rangle \Psi^{t'}(\vec{r}')\}. \tag{21}$$

The integral on d^3r on the right-hand side of Eq. (21) may be extended over all space, since by assumption $\langle r\,|U_N|\,r'\rangle = 0$ for $|\vec{r}| > R$. If we now further assume that the nuclear interaction operator is symmetric,

$$\langle \vec{r}'\,|U_N|\,\vec{r}\rangle = \langle \vec{r}\,|U_N|\,\vec{r}'\rangle, \tag{22}$$

then the entire right-hand side vanishes, since r and r' are equivalent dummy integration variables and may be interchanged in the first integrand. Local potentials [$\langle \vec{r}'\,|U_N|\,\vec{r}\rangle = U_N(\vec{r})\delta(\vec{r} - \vec{r}')$] are certainly symmetric, as are a wide class of optical potentials derived from multiple scattering theory (see Sec. IV for proof), so Eq. (22) is not unduly restrictive. The left-hand side of Eq. (21) may be transformed using vector identities and

Gauss's law, and the angular integration done by the orthonormality of the spherical harmonics. Then, assuming R is chosen so that $\chi_l^t(R)\neq 0$, divide through by $R\chi_l^{t\prime}(R)\chi_l^t(R)$ and use Eq. (18) to obtain

$$\lambda_l^t-\lambda_l^{t\prime}=2\eta kR(t-t')\int_0^R v(r)y_l^{t\prime}(r)y_l^t(r)dr\,, \quad (23)$$

where

$$y_l^t(r)\equiv r\chi_l^t(r)/R\chi_l^t(R)$$

is the radial wave function normalized to unity at the upper limit $r=R$. Finally, taking $t'=0$, $t=\pm 1$, we derive the following exact formulas for S_l and D_l:

$$S_l=\lambda_l^0+\eta kR\int_0^R v(r)y_l^0(r)[y_l^+(r)-y_l^-(r)]\,dr\,, \quad (24)$$

$$D_l=2kR\int_0^R v(r)y_l^0(r)\,\tfrac{1}{2}[y_l^+(r)+y_l^-(r)]dr\,. \quad (25)$$

All the wave functions behave near the origin as $y_l^t(r)\cong \text{const}\times r^{l+1}$ and are by definition equal at the upper limit: $y_l^+(R)=y_l^-(R)=y_l^0(R)=1$. The effect of the Coulomb potential is to give $y_l^-(r)$ slightly more curvature than $y_l^0(r)$, and $y_l^+(r)$ slightly less. Therefore it should be a good approximation in Eq. (25) to put

$$\tfrac{1}{2}[y_l^+(r)+y_l^-(r)]\cong y_l^0(r)\,. \quad (26)$$

Also, since the difference $y_l^+(r)-y_l^-(r)$ vanishes at both limits and is expected generally to be of order η, the second term in Eq. (24) is of order $\eta^2=0.0004$ and is negligible. We may therefore interpret the fit parameters S_l, D_l by the working approximations

$$S_l\cong\lambda_l^0$$
$$=R\left(\frac{\partial}{\partial r}\ln[r\chi_l^0(r)]\right)_{r=R}$$
$$=R\left.\frac{dy_l^0(r)}{dr}\right|_{r=R}\,, \quad (27)$$

$$D_l\cong 2kR\int_0^R v(r)[y_l^0(r)]^2dr\,. \quad (28)$$

For the best fitting nuclear models of Sec. IV, the error in these approximations is $\lesssim 0.2\%$ for Eq. (27), and $\lesssim 0.1\%$ for Eq. (28). Since this is well within the experimental uncertainties (Table II), Eqs. (27) and (28) are entirely adequate for our present purposes.

The general behavior S_l and D_l may be anticipated from Eqs. (27) and (28). With $v(r)$ given by Eq. (13), and the approximation $y_l^0(r)\simeq(r/R)^{l+1}$ (good for large l), Eq. (28) yields the estimate

$$D_l\simeq\frac{kR}{l+1}\left[1-(2l+1)!!\left(\frac{r_\pi^2+r_N^2}{3R^2}\right)^{l+1}\right]. \quad (29)$$

Since a more diffuse charge distribution produces a shallower potential (Fig. 1), D_l in general is a monotonically decreasing function of r_π. To increase the sensitivity of D_l to r_π, the boundary radius R should be chosen as small as possible consistent with the condition $v(r)\cong 1/r$, for $r>R$. As l increases, the integral in Eq. (28) is more dominated by the outermost values of $v(r)$, so D_l becomes both smaller and much less sensitive to r_π. It also becomes harder to measure, since S_l generally increases with l, eventually taking the form $S_l\sim l+1$, and completely dominating the D_l term in Eq. (19). It is therefore the fit parameters (S_l, D_l) for the low partial waves, especially the S

TABLE II. Model-independent fit parameters for S, P, and D waves.

p_{lab} (MeV/c)	l	Logarithmic derivative avg. and diff. (S_l, D_l) ReS_l	ImS_l	ReD_l	ImD_l	Nuclear phase shifts $\delta_l^\pm$(degrees) [a] Reδ_l^+	Imδ_l^+	Reδ_l^-	Imδ_l^-
130.2	S	-1.161 ± 0.007	-0.110 ± 0.008	4.18 ± 0.21	0.40 ± 0.24	-7.3 ± 0.2	2.2 ± 0.2	-9.0 ± 0.2	2.3 ± 0.2
142.3	S	-1.928 ± 0.008	-0.125 ± 0.008	6.07 ± 0.18	0.89 ± 0.19	-7.7 ± 0.1	1.6 ± 0.2	-9.5 ± 0.1	2.0 ± 0.1
153.2	S	-2.931 ± 0.021	-0.172 ± 0.021	9.90 ± 0.74	1.45 ± 0.74	-8.2 ± 0.3	1.5 ± 0.3	-9.7 ± 0.3	1.8 ± 0.3
163.0	S	-4.304 ± 0.034	-0.326 ± 0.033	14.67 ± 0.86	2.83 ± 0.88	-8.3 ± 0.3	1.8 ± 0.3	-10.1 ± 0.2	2.1 ± 0.2
130.2	P	0.520 ± 0.004	-0.067 [b] ±0.005	1.61 ± 0.12	0.13 [b] ±0.16	8.7 ± 0.1	1.8 ± 0.2	8.9 ± 0.1	1.9 ± 0.2
142.3	P	0.174 ± 0.004	-0.100 [b] ±0.005	2.05 ± 0.07	0.17 [b] ±0.11	10.9 ± 0.1	2.6 ± 0.1	11.1 ± 0.1	2.8 ± 0.1
153.2	P	-0.191 ± 0.007	-0.154 [b] ±0.009	2.24 ± 0.22	0.30 [b] ±0.32	12.8 ± 0.2	3.8 ± 0.3	12.6 ± 0.2	4.0 ± 0.3
163.0	P	-0.611 ± 0.007	-0.226 [b] ±0.010	2.80 ± 0.18	0.55 [b] ±0.28	14.9 ± 0.2	5.0 ± 0.3	14.7 ± 0.2	5.3 ± 0.3
130.2	D	2.100 ± 0.009	-0.013 [b] ±0.012	0.70 ± 0.29	0.02 [b] ±0.36	1.0 ± 0.1	0.1 ± 0.1	1.0 ± 0.1	0.1 ± 0.1
142.3	D	1.921 ± 0.006	-0.015 [b] ±0.007	0.78 ± 0.12	0.02 [b] ±0.16	1.5 ± 0.1	0.1 ± 0.1	1.5 ± 0.1	0.2 ± 0.1
153.2	D	1.750 ± 0.009	-0.020 [b] ±0.010	0.88 [b] $^{+0.30}_{-0.90}$	0.03 [b] ±0.25	2.0 ± 0.1	0.2 ± 0.2	2.0 ± 0.1	0.3 ± 0.2
163.0	D	1.568 ± 0.007	-0.022 [b] ±0.008	1.00 ± 0.18	0.04 [b] ±0.20	2.7 ± 0.1	0.3 ± 0.1	2.7 ± 0.1	0.3 ± 0.1

[a] Listed errors on (S_l, D_l) are the deviations that increase χ^2 by 10%. They are propagated crudely to the phase shifts via Eq. (20).

[b] These variables arbitrarily fixed at "reasonable values" in final fit (see text).

wave, that must be well determined to permit measurement of r_π. The higher partial waves need only be consistent with the general formalism. We note in passing that this formalism offers a natural way to eliminate Coulomb effects from strong-interaction cross sections: Pure nuclear phase shifts may be computed from the neutral logarithmic derivative λ_l^0 obtained from the empirical $\lambda_l^\pm$, either as their average (isoscalar targets only), or by means of an *a priori* estimate from Eq. (28) of the charge shift correction ηD_l.

Our goal here, however, is in a sense just the opposite: We want to eliminate the unknown nuclear interaction, representing it by the empirical quantities S_l. The only role left to specific models of the nuclear interaction is to generate reasonable internal wave functions $y_l^0(r)$ to use in interpreting the empirical values of D_l according to Eq. (28). The parameters of the model must be adjusted to satisfy the empirical boundary conditions of Eq. (27). Thus, no matter what nuclear model is used, the internal wave function must always be of the form Cr^{l+1} for small r, and have specified value and slope at the boundary $r=R$: $y_l(R)\equiv 1$ and $y_l'(R) = S_l/R$. These constraints on the form of y_l serve in practice to greatly reduce the sensitivity of D_l to the details of the nuclear interaction, thus providing a good separation between the strong and electrodynamic parts of the problem.

III. DATA ANALYSIS

The Berkeley data consist of measurements of the $\pi^\pm$-He elastic scattering differential cross sections $\sigma^\pm(\theta)$ at 15 scattering angles and four beam momenta: 130.2, 142.3, 153.2, and 163.0 MeV/c. The cross sections show a deep interference minimum of about 0.3–0.5 mb/sr near 70°, then rise to some 5 to 7 mb/sr in the backward direction (Fig. 2). See Ref. 3 for the full data set and details of the experiment.

From these data the fractional difference

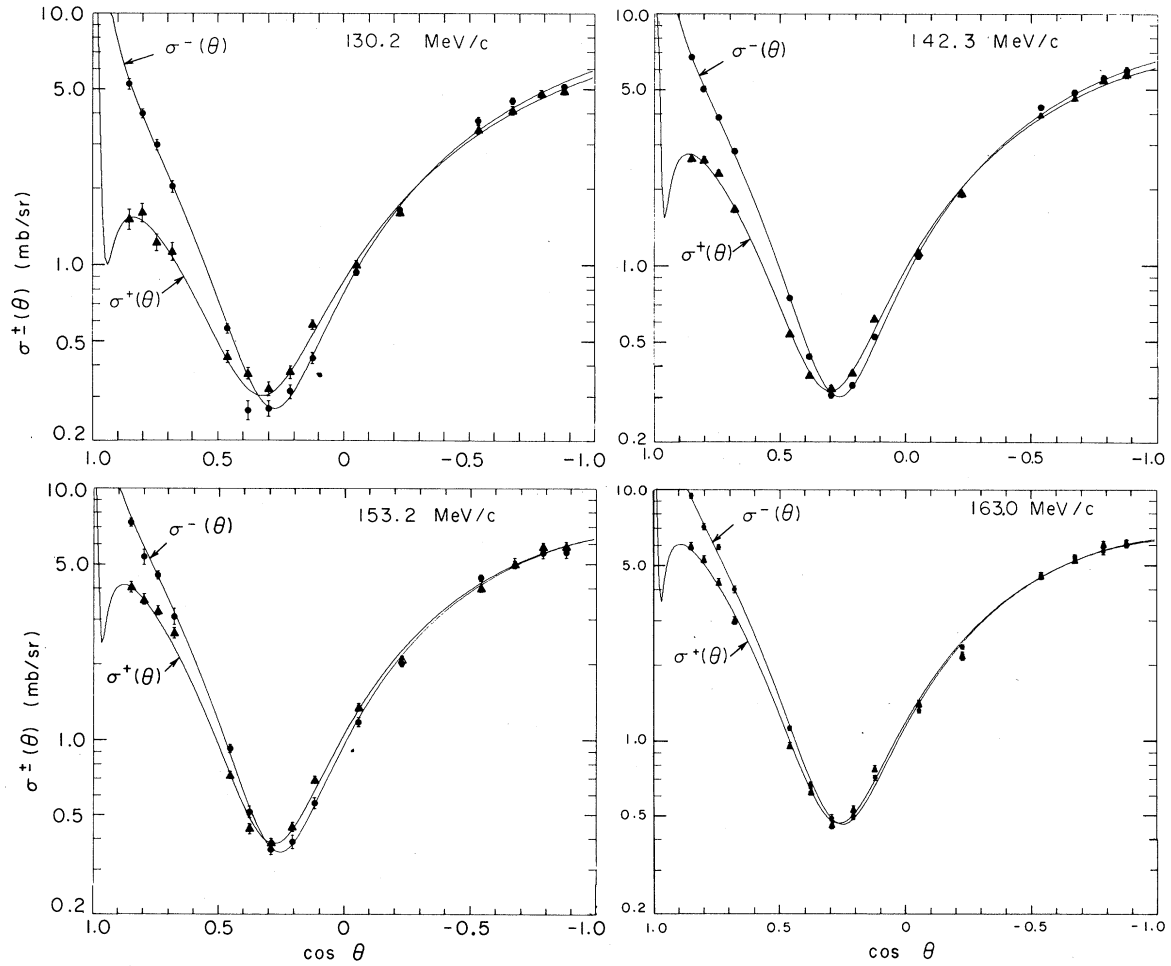

FIG. 2. Elastic differential cross sections $\sigma^\pm(\theta)$ (mb/sr) vs $\cos\theta_{c.m.}$ for $\pi^\pm$ on He^4. Theoretical curves are calculated from the model-independent-fit parameters of Table II. Triangles are π^+ data; circles are π^- data.

$$\Delta(\theta)\equiv[\sigma^-(\theta)-\sigma^+(\theta)]/\{\tfrac{1}{2}[\sigma^-(\theta)+\sigma^+(\theta)]\} \qquad (30)$$

is formed. This difference is due in general to Coulomb-nuclear interference effects, and is expected to be sensitive to the pion radius, especially near the minimum where the nuclear amplitude is small and momentum transfer is not ($q\sim 0.8$ F^{-1}). Although $\Delta(\theta)$ is not independent information, its precision benefits from the cancellation of some uncertainties in beam normalization. The total data set thus consists of 120 cross-section points $\sigma_k^{\pm}(\theta_i)$ and 60 semidependent derived quantities $\Delta_k(\theta_i)$.

The data were analyzed independently at each beam energy using Eqs. (3)–(7) and (20). To account for inelastic processes, complex values of S_l and D_l were allowed in the first three partial waves ($l\leq 2$). Higher partial waves were omitted ($a_l^{\pm}\equiv 0$ for $l>2$). The basic fitting procedure was to fix the D_l and adjust the S_l to fit the 30 cross-section points $[\sigma^{\pm}(\theta_i),\ i=1,15]$ by minimizing $\chi_+^2+\chi_-^2$ where

$$\chi_t^2=\sum_{i=1}^{15}\left(\frac{\sigma_{\rm calc}^t(\theta_i)-\sigma_{\rm data}^t(\theta_i)}{\delta\sigma(\theta_i)}\right)^2, \qquad (31)$$

and $\delta\sigma(\theta_i)$ is the experimental error. Similarly for fixed S_l, the D_l were adjusted to fit the $15\Delta(\theta_i)$ data points by minimizing the corresponding χ_Δ^2. With the improved D_l, the S_l were refitted and vice versa for as many iterations as needed until the process converged.

It was found that not all of the 12 parameters (real and imaginary parts of S_l and D_l for $l=0,1,2$) could be determined by the data. In particular, the imaginary parts were poorly constrained, since only elastic scattering data were used. Therefore only ImS_0 and ImD_0 were left free to fit the data, while the other imaginary parts were fixed at reasonable values. The choice of the "reasonable values" was guided by considerations of smooth energy dependence, unitarity (i.e., $\mathrm{Im}\delta_l^{\pm}\geq 0$), and, in the later stages, Eq. (28) for D_l with fitted optical-model wave functions. The necessity of making some such arbitrary choices is easily seen if only the main S- and P-wave amplitudes are considered, and the small Coulomb and D-wave amplitudes neglected. In that case there would be four free parameters (say, Reδ_l and Imδ_l for $l=0,1$) but, since the cross section would be quadratic in cosθ, only three coefficients could be determined by the elastic scattering data. Although our actual case is not so simple since we do have some sensitivity to the imaginary parts via interference with the Coulomb amplitude, the net empirical result is essentially that the combination $\mathrm{Im}\lambda_0+\text{const}\times\mathrm{Im}\lambda_1$ (const≈ 1.5) is well determined, while the orthogonal combination $\mathrm{Im}\lambda_0-\mathrm{Im}\lambda_1/\text{const}$ is undetermined by the data. As a check on the imaginary parts, the absorption cross section was calculated from

$$\sigma_{\rm abs}^{\pm}(k)=\frac{1}{k^2}\sum_{l=0}^{\infty}(2l+1)(1-|e^{2i\delta_l^{\pm}}|^2) \qquad (32)$$

and compared with the experimental values of Block *et al.* (Fig. 3). The fair agreement lends confidence to the choices made. In any case it is the real parts that are significant for the measurement of the pion radius, and their best-fitting values were essentially independent of the values chosen for the imaginary parts. The only constraint placed on the real parts was that in the final fit, ReD_2 for 153.2 MeV/c was fixed on a smooth curve passing through the best-fitting values of ReD_2 for the other energies. This was the only constraint necessary to give a smooth energy dependence to all the fit parameters.

Table II lists the final fit parameters (S_l, D_l) at a boundary radius of $R=3.5$ F. The corresponding phase shifts are calculated via the $a_l^{\pm}$ given by Eq. (20). Table I lists some kinematic quantities, the final χ^2 values achieved, and some indications of the relative accuracy of the four data sets. At each energy, the data were taken with all the cross-section points having roughly the same percentage experimental error $p_i\equiv\delta\sigma(\theta_i)/\sigma(\theta_i)$, so that the fractional difference data points would have roughly equal errors $\delta\Delta(\theta_i)$. The inverse rms percentage error $\bar{p}$, defined by

$$\frac{1}{\bar{p}^2}\equiv\frac{1}{N}\sum_{i=1}^{N}\frac{1}{p_i^2}, \qquad (33)$$

is given as a measure of the precision of the cross-section data. The inverse rms error $\overline{\delta\Delta}$,

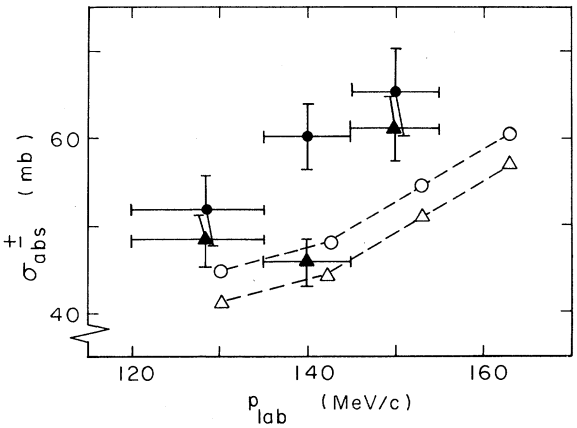

FIG. 3. Total absroption cross sections (mb) vs lab momentum (MeV/c) for π^+ (triangles) and π^- (circles). Solid symbols are data from Ref. 11, open symbols are calculated values from fit parameters of Table II.

defined similarly, specifies the average weight of the $\Delta(\theta_i)$ data points [cf. Eq. (31)], and hence the scale of the corresponding χ_Δ. It should be noted that although the 142.3-MeV/c data have the highest χ^2 values, they also have the greatest statistical precision, and in fact yield the best fits relative to the scale of their χ^2. This is also apparent in Figs. 2 and 4, where the best-fit curves calculated from Eqs. (3)–(7), (20), and (30), using the values of S_l and D_l in Table II, are shown with the data points. It should be emphasized at this point that, except for the assumption that Eq. (1) applies for $r>R$, the values given in Table II are a model-independent fit to the data. Since the differences of the logarithmic derivatives D_l are determined by fitting the $\Delta(\theta_i)$ data, the proper relationship of $\sigma^+(\theta)$ to $\sigma^-(\theta)$ is enforced in the final adjustment of the average logarithmic derivatives S_l to fit the combined $\sigma^+(\theta_i)$ and $\sigma^-(\theta_i)$ data. This constraint is absent from a conventional phase-shift analysis

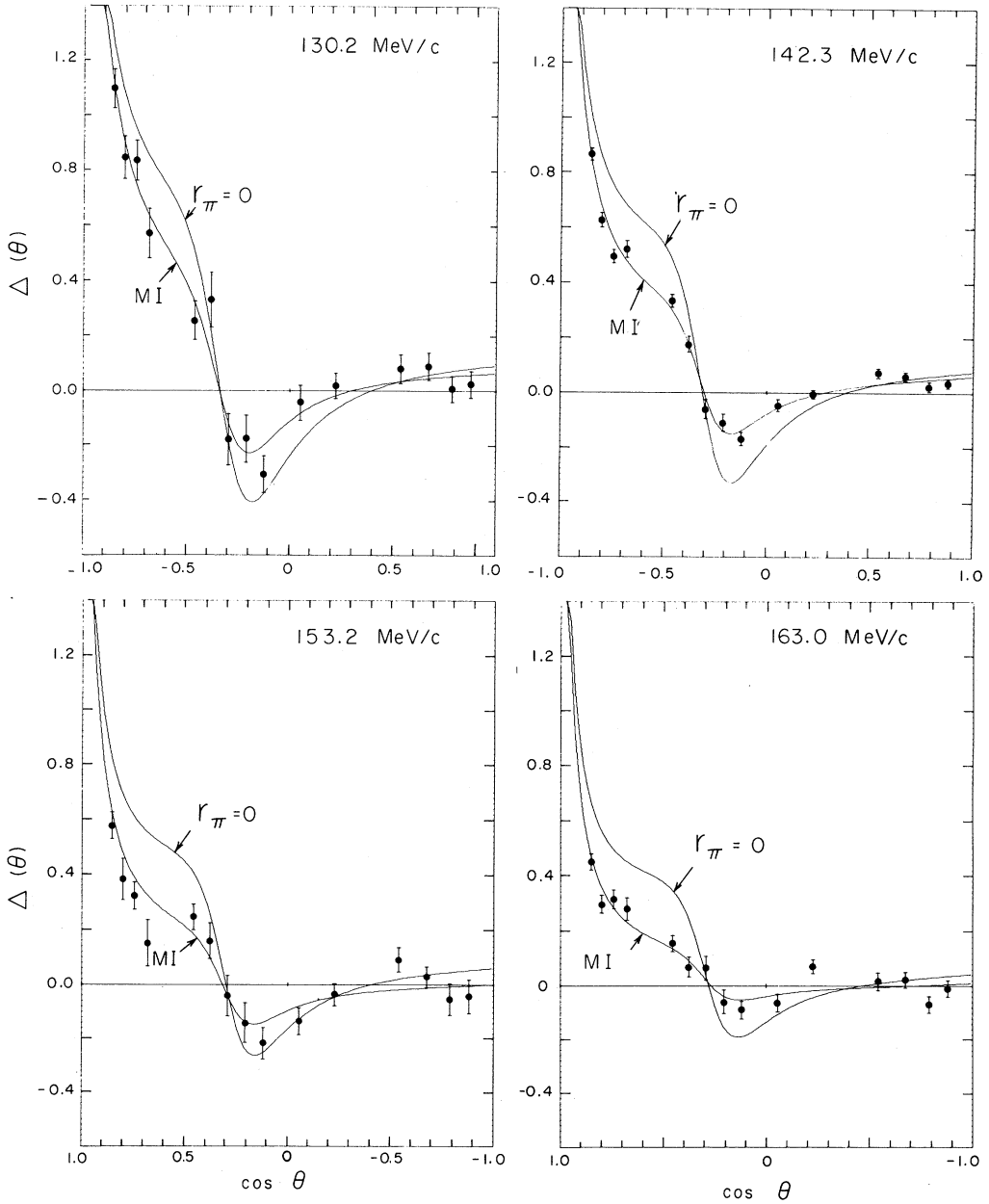

FIG. 4. Fractional difference data $\Delta(\theta)$ vs $\cos\theta_{\text{c.m.}}$. Curve *MI* calculated from model-independent-fit parameters of Table II; Curve for $r_\pi = 0$ calculated using Kisslinger-model wave functions in Eq. (28).

that separately fits the cross sections for each pion charge. Otherwise the two methods are equivalent. The fact that the resulting fit parameters show a smooth and physically reasonable energy dependence, even though each energy was analyzed separately, is viewed as further evidence in favor of these solutions.

The indicated errors in the tables are the deviations in each variable that produce a 10% increase in χ^2 with all the other variables held fixed. These are to be taken as a somewhat arbitrary, but scale-independent, measure of the relative sensitivity of the fit to the various parameters. The conventional error estimates for fitted parameters are the deviations that give unit increase in χ^2 above its minimum value, which is supposed to be less than the number of data points. This was thought inappropriate in the present case because of the mixed way the data were fitted, and because of the large χ^2 values obtained. Since we are doing a model-independent fit equivalent to a phase-shift analysis, the larger than expected χ^2 suggests underestimated data errors, possibly systematic. For example, the data points at $\theta = 80°$ consistently lie above the best-fit cross sections for both charges, and the 100° points consistently lie below. These two angles account for nearly half the total χ^2 of the $\sigma_\pm(\theta)$ fits. When the 142.3-MeV/c $\sigma_\pm$ data were refitted without them, the χ^2 improved dramatically from 112 to 48, but the fitted values of S_l hardly change (about 1%). It should be noted that this kind of systematic error, that affects both charges in the same way, tends to cancel out of the $\Delta(\theta)$ data that are used to determine the pion radius. In any case, the full data set was used in the final analysis.

IV. NUCLEAR INTERACTION MODELS

To interpret the empirical values of D_l in Table II according to Eq. (28), we need a specific form, such as the optical-model potential, for the nuclear interaction operator U_N, so that Eq. (16) can be integrated to provide a suitable internal wave function. In a multiple-scattering-theory derivation of the optical model,[19,20] the scattering wave function of a pion on a nucleus is constructed from the pion–single-nucleon scattering amplitude and properties of the nuclear states, particularly the spatial density of nucleons. The optical potential is then defined as the equivalent interaction operator, acting on pion coordinates only, that generates the same elastic scattering amplitude.

In Watson's formulation,[19] the momentum space matrix elements of the optical potential are, in the impulse approximation, and with neglect of nuclear correlations,

$$\langle \vec{k}' | U_N | \vec{k} \rangle = \frac{1}{(2\pi)^3} \int d^3x \rho(x) e^{i(\vec{k}-\vec{k}')\cdot\vec{x}} [-4\pi f(\vec{k}, \vec{k}')] . \tag{34}$$

All that remains of nuclear structure in this formula is the density of nucleons $\rho(x)$, normalized so that $\rho(x)d^3x$ is the number of nucleons in the volume element d^3x. The amplitude, averaged over spin and isospin, for any one of them to scatter the pion from incident momentum $\vec{k}$ to final momentum $\vec{k}'$ is $f(\vec{k}, \vec{k}')$. The exponential provides that each volume element contributes with the proper phase to the total amplitude.

The coordinate-space matrix elements of this optical potential are obtained by Fourier transformation. In Dirac notation [$\langle \vec{r} | \vec{k} \rangle = (2\pi)^{-3/2} e^{i\vec{k}\cdot\vec{r}}$], we have

$$\langle \vec{r}' | U_N | \vec{r} \rangle = -4\pi \int d^3x \rho(\vec{x}) \int d^3k \int d^3k' f(\vec{k}, \vec{k}') \times \langle \vec{r}' | \vec{k}' \rangle \langle \vec{k}' | \vec{x} \rangle \langle \vec{x} | \vec{k} \rangle \langle \vec{k} | \vec{r} \rangle . \tag{35}$$

Since $\langle \vec{k} | \vec{r} \rangle = \langle \vec{r} | \vec{k} \rangle^* = \langle \vec{r} | -\vec{k} \rangle$, and $\vec{k}$ and $\vec{k}'$ are dummy integration variables, we see by inspection that $\langle \vec{r}' | U_N | \vec{r} \rangle$ satisfies the symmetry condition of Eq. (22) provided

$$f(-\vec{k}', -\vec{k}) = f(\vec{k}, \vec{k}') . \tag{36}$$

In terms of a partial-wave expansion

$$f(\vec{k}, \vec{k}') = \sum_{l=0}^{\infty} (2l+1) a_l(k, k') P_l(\hat{k}' \cdot \hat{k}) \quad \text{with } k \equiv |\vec{k}|, \quad \hat{k} \equiv \vec{k}/k ; \tag{37}$$

this only requires that the partial-wave amplitudes be symmetric in k and k':

$$a_l(k, k') = a_l(k', k) . \tag{38}$$

This is trivially satisfied on the energy shell where $k = k'$. Thus the symmetry condition of Eq. (22), which is essential to the derivation of the key equations (27) and (28), is translated in the optical-model formalism into a symmetry condition Eq. (38) on the off-shell behavior of the pion-nucleon partial-wave amplitudes. In Eq. (36), this condition takes the form of an off-shell extrapolation of time-reversal invariance.

Kisslinger's optical potential is a convenient and widely used approximation to Eqs. (34) through (37). It consists of keeping only the first two partial waves of Eq. (37) in the form[21]

$$-4\pi f(\vec{k}, \vec{k}') \cong b + c\vec{k}' \cdot \vec{k} , \tag{39}$$

where b and c are certain linear combinations of the S- and P-wave scattering lengths. All of the

integrations in Eq. (35) may then be done explicitly, yielding the form

$$\langle \vec{r} | U_N | \Psi \rangle = b\rho(\vec{r})\Psi(\vec{r}) - c\vec{\nabla} \cdot (\rho(\vec{r})\vec{\nabla}\Psi(\vec{r})) \qquad (40)$$

for the right-hand side of Eq. (16). The local nuclear interaction potential $U(r) \equiv b\rho(r)$ is repulsive and dominates the S wave. The nonlocal interaction operator $-\vec{\nabla} \cdot \alpha(r)\vec{\nabla}$, with $\alpha(r) \equiv c\rho(r)$, is attractive and dominates all higher partial waves. This explanation of the observed behavior of pion-nucleus interactions is the principal achievement of the Kisslinger model. Substitution of Eqs. (40) and (17) into Eq. (16) results in the radial Eqs. (A1) and (B1) of the appendixes. Ericson and Ericson have refined the model, taking into account more details of nuclear structure and pion-nucleon interactions, but finding the same general form of wave equation.[20]

We assume the He^4 nucleon density has the same Gaussian form [Eq. (11a)] and extent ($a_N = 1.34$ F) as the He^4 charge density (Fig. 1). For our purposes, $b \equiv b_1 + ib_2$ and $c \equiv c_1 + ic_2$ may be considered complex phenomenological constants to be determined by the data. In particular, an attempt was made, using the methods of Appendix B, to adjust b and c so that the numerically computed λ_l^0 would match the experimental S_l [Eq. (27)], at least for the S and P waves. This proved impossible, however, due to a branch cut in $\lambda_l^0(b, c)$ along the negative real axis $[-\infty < c_1 < -\rho(0)^{-1}]$ of the complex c plane. As c_2 passed through zero in the search routine, $\mathrm{Im}\lambda_1$ jumped from a value well below the empirical $\mathrm{Im}S_1$ to a value well above it. This discontinuity is shown in Appendix A to result from the singular point r_0 in the Kisslinger-model radial equation where $\alpha(r_0) = -1$. The wave function in general has a logarithmic branch point at r_0. For $c_2 = 0$ this is in the nuclear surface where the density has fallen to the value $\rho(r_0) = -1/c_1$. If $c_2 \neq 0$, r_0 moves slightly off the real r axis, and the sign of c_2 determines which branch of the function is generated. Consequently, the computed logarithmic derivatives, and corresponding nuclear phase shifts, may have intrinsic imaginary parts even in the limit of real b and c. This effect obviously ruins the interpretation of b_2 and c_2 as a measure of physical pion absorption processes in nuclear matter.

This unphysical behavior is evidently a consequence of integrating the low-energy approximation (39) over all momentum space in the course of the Fourier inversion leading to Eq. (40). In fact, Lepore and Riddell have shown, by direct numerical solution of the partial-wave Schrödinger equation in momentum space for the optical-model interaction (34), that the singular-point effects in the wave function disappear if the coefficients (b, c) of Eq. (39) are given a gradual cutoff for large k and k'.[22] All of this is a serious difficulty in principle with the Kisslinger model: The wave functions it generates, having logarithmic branch points, cannot be physically correct.

For our present purposes, however, all we really require is a set of radial wave functions $\chi_l^0(r)$ $(l = 0, 1, 2)$ satisfying the boundary conditions $\lambda_l^0 = S_l$, to be used to interpret the empirical D_l's according to Eq. (28). To this end, we have adopted the following *ad hoc* procedure. The imaginary part of the P-wave logarithmic derivative, $\mathrm{Im}S_1$, was temporarily replaced by a fake value $\mathrm{Im}S_1'$ large enough to permit a solution for (b, c) that satisfies the corresponding modified S and P wave boundary conditions. The result is given in the first three columns of Table III. Then with c fixed at the value so determined, the complex parameter b was readjusted separately for each partial wave to exactly satisfy the original empirical boundary conditions. For the S wave there was, of course, no change in b. For the P and D waves we find $b_2 > 0$, to partially cancel the anomalously large negative $\mathrm{Im}S_l$ resulting from the singular point. These values are given in the last two columns of Table III. We refer to this solution in Sec. V as the "modified Kisslinger model." At 142.3 MeV/c, a fit was also done with $a_N = 1.27$ F as a check on the sensitivity to nuclear density. This solution is listed in the Tables as data set b'. The solid curves in Fig. 5 show the real part of the fitted weighting functions

TABLE III. Modified Kisslinger-model optical parameters.

Data set [a]	Fake $\mathrm{Im}S_1$	c(F^3)	Readjusted local const b (F)		
			S wave	P wave	D wave
a	−0.13	$-6.40 - 0.16i$	$1.24 - 0.26i$	$1.16 + 0.41i$	$3.15 + 0.22i$
b	−0.19	$-6.62 - 0.25i$	$1.37 - 0.15i$	$1.87 + 0.59i$	$3.42 + 0.59i$
b'	−0.19	$-6.14 - 0.10i$	$1.28 - 0.17i$	$1.82 + 0.61i$	$2.27 + 0.66i$
c	−0.25	$-6.61 - 0.26i$	$1.50 - 0.07i$	$1.98 + 0.53i$	$3.79 + 0.47i$
d	−0.35	$-6.78 - 0.15i$	$1.65 - 0.04i$	$2.20 + 0.50i$	$4.10 + 0.41i$

[a] Model b' has density radius parameter $a_N = 1.27$ F [cf. Eq. (11b)]. The rest have $a_N = 1.34$ F.

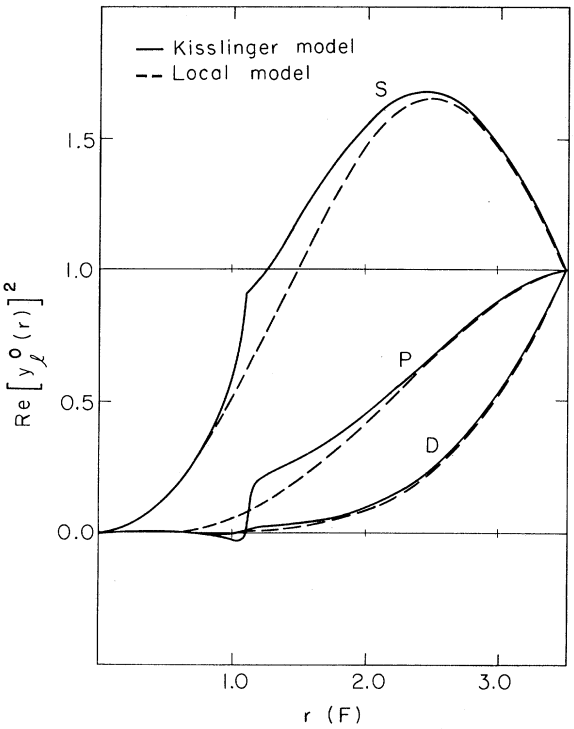

FIG. 5. Real part of normalized weighting functions $[y_l^0(r)]^2 = [r\chi_l^0(r)/R\chi_l^0(R)]^2$ for S, P, and D waves at 142.3 MeV/c lab momentum. Solid curves for modified Kisslinger model, dashed curves for local potential model.

$$[y_l^0(r)]^2 \equiv [r\chi_l^0(r)/R\chi_l^0(R)]^2 \tag{41}$$

resulting from this model. The peculiar behavior near $r = 1.1$ F is the remnant of a sharp spike in $\chi_l^0(r)$ at the singular point; it appears considerably damped by the normalizing condition $y_l^0(R) \equiv 1$.

As a simple alternative to test nuclear model dependence, the same programs with $c \equiv 0$ were used to fit a different complex local potential $U_l(r) = b_l\rho(r)$ to each partial wave. The results are listed in Table IV. This completely *ad hoc* model, also used for similar purposes by Block *et al.*,[11] is loose enough to fit any data. The weighting functions it generates, shown by the dashed curves in Fig. 5, are well behaved, and perhaps thereby more realistic than those of the modified Kisslinger model.

V. DETERMINATION OF THE PION RADIUS

Given an internal wave function $y_l^0(r)$ that satisfies the boundary conditions, and a formula such as Eq. (13) or (15) for the internal Coulomb potential $v(r)$, we may calculate D_l as a function of r_π. Since we have two nuclear models (Kisslinger and local) and two pion shapes (Gaussian and Yukawa), there are four cases to consider. Figure

TABLE IV. Local-model optical parameters ($c \equiv 0$).

Data set	Adjusted b_l (F) S wave	P wave	D wave
a	$1.08 - 0.34i$	$-6.47 - 0.92i$	$-12.31 - 0.90i$
b	$1.10 - 0.26i$	$-6.59 - 1.10i$	$-12.70 - 0.92i$
b'	$1.07 - 0.26i$	$-6.78 - 1.08i$	$-14.30 - 0.99i$
c	$1.12 - 0.23i$	$-6.58 - 1.36i$	$-12.39 - 1.12i$
d	$1.13 - 0.27i$	$-6.75 - 1.56i$	$-12.67 - 1.10i$

6 shows the calculated $\mathrm{Re}D_l$ vs r_π at 142.3 MeV/c for the first three partial waves. The calculated curves for free waves [i.e., $\chi_l(r) = j_l(kr)$, the spherical Bessel function] are also included to show the effect of wave-function distortion by the nuclear force. The nuclear force is repulsive in the S wave, attractive in higher waves. This results in a decrease in $\mathrm{Re}D_0$ and an increase in $\mathrm{Re}D_l$ for $l \geq 1$ from their free-wave values. To show the dependence on the pion model, the S-wave curves are drawn for both pion charge distributions. The two distributions are of course

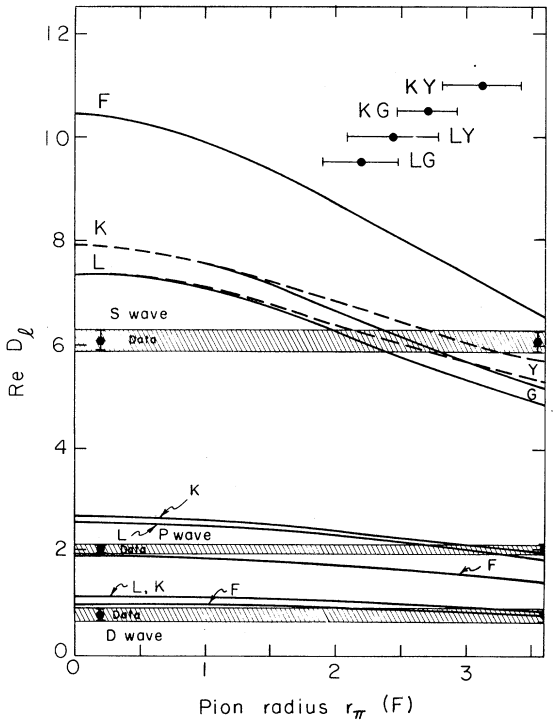

FIG. 6. $\mathrm{Re}D_l$ vs $r_\pi(F)$ for S, P, and D waves at 142.3 MeV/c (data set b). Horizontal bands are data values and errors from model-independent fit (Table II). Solid curves (G) calculated from Eq. (28) with Gaussian pion charge distribution using wave functions generated by local (L) and Kisslinger (K) nuclear interaction models. Curves for free-particle wave functions (F) are shown for comparison. Dashed curves (Y) are for Yukawa pion model [Eq. (15)]. The "data points" are the fitted pion radii and errors from Table V.

identical at $r_\pi = 0$, but for large pion radius, the Yukawa model [Eq. (15)] gives the larger value of D_l, corresponding to a deeper central value of the Coulomb potential. The effect of the nuclear model on the calculated values of D_l is also exhibited. For the same internal Coulomb potential, the modified Kisslinger-model wave function yields a value of $\mathrm{Re}D_0$ some 6% larger than the local model. For the P and D waves, where the internal wave function is more dominated by the centrifugal potential, the nuclear model dependence of $\mathrm{Re}D_l$ is 2.8% and 1.6%, respectively.

The horizontal bands are the empirical values of $\mathrm{Re}D_l$ from Table II, with the deviations that cause a 10% increase in χ_Δ^2. The pion radius for each model may be read from the intersection of the computed curve for $\mathrm{Re}D_0$ with the data band. This indicates a surprisingly large pion radius of between 2 and 3 F. With the pion radius so determined, the calculated $\mathrm{Re}D_l$ for the P and D waves lies somewhat above the corresponding data bands. Nevertheless, the numerical agreement is close enough to be taken as some confirmation of the basic equations (27) and (28). Note that without the wave-function distortion by the nuclear force, there would be no agreement on the value of r_π among the partial waves.

For a data fit completely consistent with a given model, we compute D_l for all partial waves as a function of pion radius, and using the empirical values of S_l from Table II, we plot χ_Δ^2 vs r_π (Fig. 7). The values of χ_Δ^2 and r_π at the minima, with the deviations Δr_π that cause a 10% increase in χ_Δ^2 for the various models, are listed in Table V. Some of these values of r_π are also shown in Fig. 6. The minimum values of χ_Δ^2 are larger than for the model-independent fit of Table II because of the additional constraint: The P wave is well determined by the precise data in the minimum, and it disagrees slightly with the calculated value for each model. The following remarks may be made about Fig. 6 and Table V:

(i) The 142.3-MeV/c data again have the highest χ_Δ^2 (around 60 for 15 data points), but have the sharpest minima, reflected in the size of the Δr_π.

(ii) The modified Kisslinger model gives pion radii about 0.4–0.6 F larger than the local model with the same pion form. Since the wave functions generated by these two models are about as different as possible within the constraints imposed by the boundary conditions at $r = 0$ and $r = R$, we may estimate that the uncertainty in r_π due to the nuclear model dependence is $\lesssim 0.6$ F.

(iii) In the 2 to 3 F range, with a given nuclear model, the Yukawa pion model indicates an r_π about 0.2–0.5 F bigger than the Gaussian pion model. This is a measure of the uncertainty in r_π due to choice of pion shape.

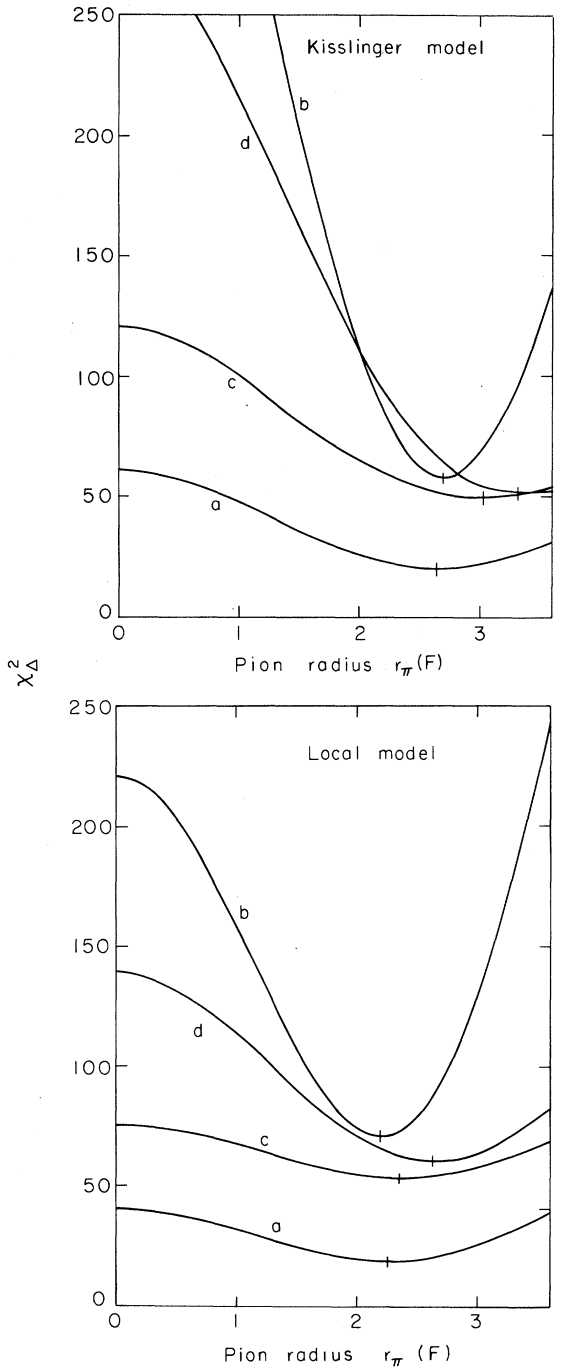

FIG. 7. χ_Δ^2 vs $r_\pi(F)$ for Gaussian pion model and both nuclear models. Labels a, b, c, d refer to the data sets at the four beam momenta (cf. Table I).

(iv) All four energies are consistent, with perhaps a slight tendency for the higher energies to require a bigger r_π to fit.

Figure 4 shows the data and calculated values of $\Delta(\theta)$ at each energy for the best model-independent

TABLE V. Pion radii from minimizing χ_Δ^2 for various models.

Data set	Modified Kisslinger nuclear model				l-dependent local potential nuclear model			
	Gaussian		Yukawa		Gaussian		Yukawa	
	r_π [a] Δr_π	χ_Δ^2	r_π Δr_π	χ_Δ^2	r_π Δr_π	χ_Δ^2	r_π Δr_π	χ_Δ^2
a	2.64±0.39	19.9	3.02±0.51	19.2	2.26±0.41	19.0	2.52±0.51	18.4
b	2.70±0.23	58.2	3.12±0.30	52.0	2.19±0.29	71.5	2.44±0.35	66.0
b'	2.63±0.25	64.9	3.02±0.32	57.8	2.21±0.30	77.9	2.47±0.37	71.8
c	3.03±0.61	49.6	3.61±0.82	46.3	2.35±0.72	53.6	2.71±0.89	50.7
d	3.32±0.42	51.9	4.02±0.57	47.7	2.63±0.50	60.6	3.05±0.64	56.0

[a] All radii in F. Gaussian model uses Eq. (13), Yukawa model uses Eq. (15).

fits (Table II). The curves for the best model-dependent fits (Tables III, IV, and V) are very similar, although they give somewhat higher χ^2 values. The curves for $r_\pi = 0$ calculated with the fitted Kisslinger-model wave functions are shown for comparison. These gave the highest calculated χ^2 values (cf. Fig. 7). All this shows that $\Delta(\theta)$ is too small in the forward direction, or correspondingly, that $\sigma^+(\theta)$ is too close to $\sigma^-(\theta)$ to permit a small value of r_π.

VI. DISCUSSION OF ALTERNATIVES

Within our basic assumption that the Coulomb potential, Eq. (10), is the only charge-dependent interaction in the generalized Klein-Gordon equation (16), data analysis indicates a surprisingly large r_π of 2 to 3 F. The boundary-condition method effectively reduces the uncertainty in r_π due to nuclear model dependence to about the level of the uncertainty due to experimental statistics. The use of the exact external ($r > R$) solution of the radial wave equation avoids the long-range Coulomb divergence difficulties. Evidently then, the large-pion-radius result is inherent in the data and our basic theoretical assumption [Eqs. (10) and (16)], and is not due to either calculational difficulties or the detailed choice of nuclear interaction model. In view of the disagreement with the simple vector-dominance-model prediction of $r_\pi = 0.63$ F, some comments are in order on possible alternative methods and assumptions:

(i) A direct optical-model analysis requires at least six numerical integrations (for $\chi_l^\pm$, $l = 0, 1, 2$) for each iteration of the search routine that adjusts the parameters of the model (including r_π) to fit the scattering data. Since only solutions consistent with the given model are considered, the question of model dependence of the results is left open. However the arguments of Sec. II are valid for a very general class of nuclear models, and imply that the result for r_π is not sensitive to the particular model used. Any model flexible enough to fit the data should yield the same phase shifts, and thereby generate wave functions that satisfy, at least implicitly, our key equations (27) and (28). Our *ad hoc* adjustment of each partial wave to fit the empirical boundary conditions guarantees this flexibility at the cost of giving up a simple physical interpretation of the nuclear parameters. Partly due to the singular-point difficulty (Sec. IV), the Kisslinger model without this *ad hoc* adjustment is not quite capable of an optimum data fit.

(ii) In order to provide a more efficient and model-independent analysis, Schiff[5] proposed evaluating the Coulomb perturbations on the dominant strong-interaction amplitude to first order in the small parameter $\eta \simeq 0.02$. Writing $\sigma^\pm(\theta) \equiv |f^\pm(\theta)|^2$, and neglecting terms of order η^2, we have

$$f_{\rm av} \equiv \tfrac{1}{2}(f^+ + f^-) = f_N^0 , \tag{42}$$

the pure strong-interaction amplitude given in general by Eq. (5) with $t = 0$. The Coulomb difference in general may be written

$$f_\Delta \equiv \tfrac{1}{2}(f^+ - f^-) = f_B + f_D , \tag{43}$$

where $f_B \equiv -2\eta k F_\pi(q) F_N(q)/q^2$ is the Coulomb–Born term depending directly on the form factors, and f_D is an additional "distortion amplitude" due to deformation of the Coulomb wave functions by the nuclear force. Although f_D for a given model is well defined in nonforward directions by Eq. (43), it diverges as q^{-2} for $q \to 0$. Schiff showed that the partial-wave expansion of f_D is correspondingly plagued by the logarithmic divergences characteristic of $1/r$ potentials, whether they act on free spherical waves or nuclear phase shifted ones. Subsequent authors[7-12] have discussed methods for handling these divergences, but Crowe *et al.* find inconsistent results when the various prescriptions are applied to their data.[23] As might be expected from the divergence problems, f_D seems to be determined mainly by the nuclear phase shifts δ_l^0, and is relatively insensitive to other details of the model,[2] including r_π. These long-range Coulomb distortion effects are thus automatically accounted for in a direct optical-model calculation, and more

generally in our boundary condition method, by the use of the exact external phase-shifted Coulomb radial wave functions [Eq. (2)].

(iii) We have taken relativity explicitly into account only in the kinematics used to calculate k and η. Only the instantaneous (Coulomb-gauge) electrostatic potential is included in the equation of motion. The magnetic field seen in the c.m. system due to the recoil motion of the nucleus is neglected. Rix and Thaler[24] suggest that k and η be chosen for the relativistic two-body problem so that the pure Coulomb amplitude, Eq. (4), agrees to first order with the covariant Feynman–Born amplitude for the electromagnetic interaction of two spinless bosons. This leads to

$$2k\eta = 2Ze^2(E_1E_2 + k^2)/(E_1 + E_2),$$

where E_1, E_2 are the c.m. energies of the two particles, and k is the c.m. momentum. Our formula differs only in the absence of the k^2 term from the numerator. (This k^2 term presumably represents the magnetic contribution.) Another alternative would be to neglect nuclear recoil motion, and use the lab momentum and velocity of the pion to compute (k, η). Magnetic interaction would then be strictly zero, and the Klein-Gordon equation in a Coulomb field would govern the long-range motion of the pion. Both these alternatives give a value of η about 2–3% larger than ours, and lead ultimately to a small increase in the measured value of r_π.

(iv) Christensen[13] attempts to calculate the distortion amplitude using conventional Feynman-diagram techniques for the electromagnetic corrections to the strong π-α amplitude. After numerous approximations and simplifying assumptions, he concludes that certain crossed diagrams ("relativistic terms"), which are omitted in a calculation based on a wave equation, can contribute to the distortion amplitude in such a way as to allow a fit to the data with smaller r_π, more in the expected range $r_\pi < 1.0$ F. He points out, however, that this result is sensitive to such details of the strong-interaction amplitude as its off-mass-shell behavior, for which he uses a linear approximation, and its over-all phase, which he leaves arbitrary. But this angle-dependent phase, which is determined implicitly by the phase shifts in the other formulations of the problem, is crucial to the Coulomb-nuclear interference effects used to determine r_π. This only serves to reemphasize the need for an accurate model with well controlled approximations to extract the small pion size effects from this kind of data.

(v) The assumption of exact charge independence of the nuclear interaction operator is crucial to this whole approach to the measurement of r_π. If the nuclear interaction of π^+ differed slightly from that of π^-, there would be a direct strong-interaction contribution to the logarithmic derivative difference D_l [Eq. (19)]. Let $U_N^\pm$ be the nuclear interaction operator for $\pi^\pm$, and assume that the difference $\Delta U_N \equiv U_N^+ - U_N^-$ is a local operator. Then, by the derivation leading to Eq. (28), we have $D_l \to D_l^C(r_\pi) + D_l^S$, where $D_l^C(r_\pi)$ is the pion-radius-dependent Coulomb contribution given by Eq. (28), and D_l^S is an additional strong charge-asymmetry contribution given by

$$D_l^S = \frac{R}{2\eta}\int_0^R \Delta U_N(r)[y_l^0(r)]^2 dr\,. \tag{44}$$

The experimental values of D_l from Table II are now to be interpreted according to

$$D_l^{\text{Expt}} = D_l^C(r_\pi) + D_l^S\,. \tag{45}$$

Any combination of r_π and ΔU_N that satisfies Eq. (45) [via Eqs. (28) and (44)] will agree with the data. The values of r_π given in Table V are based on the assumption that $D_l^S = 0$. Since D_l^C is a decreasing function of r_π (Fig. 6), we require in general $D_l^S \leq 0$ $(U_N^+ \leq U_N^-)$ to fit the data with smaller values of r_π. For example, using the local model wave functions, it would require $\mathrm{Re}D_0^S \cong -1.13$ to bring the 142.3-MeV/c S-wave data into agreement with $r_\pi = 0.63$ F. Evaluation of Eq. (44) on the assumption that $U_N^\pm(r) = (b \pm \frac{1}{2}\Delta b)\rho(a_N; r)$, where $b = 1.1$ F from Table IV, and $\rho(a_N; r)$ is given by Eq. (11), then leads to a fractional strength difference $\Delta b/b = +0.073$ $D_0^S = -0.083$. Similarly, if $U_N^\pm(r) = b\rho(a_N \pm \frac{1}{2}\Delta a; r)$,[25] we have to lowest order a fractional range difference $\Delta a/a_N \cong -0.10$ $D_0^S = +0.113$. At least for these simple models, then, roughly a 10% violation of strong-interaction charge independence is required to bring our fit into agreement with the vector-dominance-model prediction for r_π.

(vi) Finally, Oades *et al.*[14] use a boundary condition method similar to ours, but with more simplifying approximations, to calculate first-order Coulomb corrections to the phase shifts. On applying their analysis to the Berkeley data, they find somewhat larger r_π and χ^2 than we do. They also find that the other $\pi^\pm$-He^4 data,[6,11] although in some disagreement with the Berkeley data, are not precise enough to show much sensitivity to r_π; it is consistent with any $r_\pi < 2.2$ F. In view of this conflict and uncertainty in the data, and the availability of workable methods of analysis, another precision measurement of $\pi^\pm$ scattering on an isoscalar target appears worthwhile. If such experiments confirm the large pion charge radius, no matter what the ultimate cause, it is signifi-

cant for the calculation of Coulomb corrections in pion nuclear scattering and pionic atoms in general.

ACKNOWLEDGMENTS

I would like to express my appreciation to Dr. R. J. Riddell, Jr. for the initial suggestion and extensive advice, support, and encouragement in the course of this work; to Dr. K. M. Crowe, A. Fainberg, and Dr. A. S. L. Parsons for many very useful discussions and the use of their data in advance of publication; and to Dr. J. V. Lepore for numerous helpful conversations.

APPENDIX A: ANALYSIS OF THE KISSLINGER-MODEL SINGULAR POINT FOR REAL $\alpha(r)$

The radial Schrödinger equation for the Kisslinger model of pion-nucleus interactions has the general form

$$\frac{d}{dr}\left(r^2[1+\alpha(r)]\frac{d\chi}{dr}\right) + \{r^2[k^2-U(r)]-[1+\alpha(r)]l(l+1)\}\chi=0\,. \tag{A1}$$

The complex nonlocal interaction coefficient $\alpha(r)$ is in general proportional to the nuclear density $\rho(r)$, and vanishes outside the nucleus. We take for simplicity $\alpha(r)=c\rho(r)$ where $c=c_1+ic_2$ is a complex constant. The essential features of the following argument remain valid, however, for more complicated forms of $\alpha(r)$ such as those given in Ref. 20. Equation (1) has a singular point r_0 where $1+\alpha(r_0)=0$. If $c_2=0$ and $\alpha(0)=c_1\rho(0)<-1$, this singular point will be in the nuclear surface where the density has fallen to the value $\rho(r_0)=-1/c_1$. If $c_2\neq 0$, the singular point will be at the complex value of r_0 where $\rho(r_0)=-1/c=(-c_1+ic_2)/|c|^2$. For the Gaussian density distribution, and presumably in general, $\mathrm{Im}r_0$ has the opposite sign from c_2: For $c_2<0$, r_0 lies above the real r axis, and comes down onto the axis as $c_2\to 0$.

To investigate the effect of this singular point on the Kisslinger radial wave function, we apply the classical analysis of second-order linear differential equations as given in Ref. 26. Writing the radial equation in the form

$$\chi''+p(r)\chi'+q(r)\chi=0\,, \tag{A2}$$

we find that both

$$p(r)\equiv\frac{2}{r}+\frac{\alpha'(r)}{1+\alpha(r)}$$

and

$$q(r)\equiv\frac{k^2-U(r)}{1+\alpha(r)}-\frac{l(l+1)}{r^2} \tag{A3}$$

have first-order poles at $r=r_0$. Substitution of power-series expansions about r_0 for $(r-r_0)p(r)$ and $(r-r_0)^2q(r)$, and the form

$$y(r)=(r-r_0)^\beta\left[1+\sum_{m=1}^{\infty}a_m(r-r_0)^n\right] \tag{A4}$$

for χ into Eq. (A2) then yields a set of recursion formulas for the a_n. The first of these is the indicial equation which turns out to be $\beta^2=0$. Therefore $y(r)$ is analytic at r_0:

$$y(r)=1+a_1(r-r_0)+a_2(r-r_0)^2+\cdots\,, \tag{A5}$$

and, since the indicial equation has equal roots, the second independent solution must be sought by variation of parameters. Writing it in the form $w(r)=\xi(r)y(r)$, we find on substitution in Eq. (A2) that

$$\frac{d\xi}{dr}=\frac{1}{r^2[1+\alpha(r)]y^2(r)}\,. \tag{A6}$$

This means that since $1+\alpha(r)$ has a simple zero at r_0, $\xi'(r)$ has a simple pole there, and $\xi(r)$ has a logarithmic branch point. The general solution of Eq. (A2),

$$\chi(r)=[A+B\xi(r)]y(r)\,, \tag{A7}$$

where A and B are arbitrary constants, then also has a logarithmic branch point at r_0 (unless $B=0$). Now the physical solution of the radial equation must start at the origin as $\chi(r)\simeq\mathrm{const}\times r^l$. We want to propagate this solution outward along the real r axis to the boundary $r=R$, using the form (A7) to cross the singular point. The constants (A,B) are determined by the continuity of $\chi(r)$ and $\Psi(r)\equiv r^2[1+\alpha]\chi'(r)$ at $r=r_1\equiv r_0-\Delta r$:

$$\begin{aligned} B&=y(r_1)\Psi(r_1)-r_1^2[1+\alpha(r_1)]y'(r_1)\chi(r_1)\,,\\ A&=\chi(r_1)/y(r_1)-B\xi(r_1)\,. \end{aligned} \tag{A8}$$

Since $y(r)$ and $\chi(r)$ both satisfy Eq. (A2), B is actually independent of r_1. The same continuity conditions are used again at $r=r_2\equiv r_0+\Delta r$ to obtain the values of $\chi(r_2),\Psi(r_2)$ needed to continue the integration:

$$\begin{aligned} \chi(r_2)&=\frac{y(r_2)}{y(r_1)}\chi(r_1)+y(r_2)B[\xi(r_2)-\xi(r_1)]\,,\\ \Psi(r_2)&=\frac{1}{y(r_2)}\{B+r_2^2[1+\alpha(r_2)]y'(r_2)\chi(r_2)\}\,. \end{aligned} \tag{A9}$$

We therefore must somehow evaluate the singular integral

$$I(\Delta r) \equiv \xi(r_2) - \xi(r_1) \equiv \int_{r_0-\Delta r}^{r_0+\Delta r} \frac{dr}{r^2[1+\alpha(r)]y(r)^2} . \quad \text{(A10)}$$

The pole at $r = r_0$ may be explicitly separated by a partial-fraction expansion of the integrand. Writing the denominator in the form (with $z = r - r_0$)

$$r^2[1+\alpha(r)]y(r)^2 \equiv z[g + zh(z)], \quad \text{(A11)}$$

we have $g = r_0^2\alpha'(r_0)$ and $h(z) = h_0 + h_1 z + h_2 z^2 + \cdots$, where

$$h_0 = 2r_0^2\left[\frac{\alpha'(r_0)}{r_0} + U(r_0) - k^2 + \tfrac{1}{4}\alpha''(r_0)\right], \quad \text{etc.} \quad \text{(A12)}$$

Then

$$I(\Delta r) = \frac{1}{g}\int_{-\Delta r}^{+\Delta r}\left(\frac{1}{z} - \frac{h(z)}{g + zh(z)}\right)dz = I_1 + I_2(\Delta r) . \quad \text{(A13)}$$

The second integral, $I_2(\Delta r)$, is a dull, well-behaved function of Δr. To lowest order in r it is

$$I_2(\Delta r) \simeq -\frac{2h_0}{g^2}\Delta r + O((\Delta r)^3) . \quad \text{(A14)}$$

To evaluate I_1 however, we must detour around the pole in the integrand. For a continuation of the solution when the pole is above the axis ($c_2 < 0$), we use the z-plane contour shown in Fig. 8. Then $I_1 = +i\pi/g$. Similarly, for a continuation of the solution when $c_2 > 0$, we must go above the pole. This yields $I_1 = -i\pi/g$. Substituting all this back into Eq. (A9), and expanding everything to lowest order in Δr, we have

$$\chi(r_2) = \chi(r_1) \pm \frac{i\pi}{g}\Psi(r_1) + 2\Delta r\left[a_1(1 \pm i\tfrac{1}{2}\pi)\chi(r_1) + \frac{h_0}{g}\Psi(r_1)\right] + \cdots , \quad \text{(A15)}$$

$$\Psi(r_2) = \Psi(r_1) + 2a_1\Delta r[(-1 \pm i\tfrac{1}{2}\pi)\Psi(r_1) + g\chi(r_1)] + \cdots ,$$

where the upper sign corresponds to continuation from negative c_2, and

$$a_1 = [U(r_0) - k^2]/\alpha'(r_0) .$$

Thus even if the radial wave function $\chi(r)$ started off real for small r, as it could if the optical potentials $[U(r), \alpha(r)]$ were real, it would develop an imaginary part on propagation through the singular point r_0. Consequently the logarithmic derivative at the boundary $R > r_0$, defined by

$$\lambda(R) \equiv 1 + \Psi(R)/R\chi(R) ,$$

will be complex even in the limit of a real optical potential. And since the sign of its imaginary part depends on whether c_2 approaches zero from above or below, $\mathrm{Im}\lambda(R)$ will have a discontinuity at $c_2 = 0$. If we let $U(r) = b\rho(r)$, and consider $\lambda(R)$ as a function of the two complex variables $b = b_1 + ib_2$ and $c = c_1 + ic_2$, we have in general $\lambda(b^*, c^*) = \lambda^*(b, c)$. This implies that when the local potential is complex ($b_2 \neq 0$), $\mathrm{Re}\lambda(R)$ also develops a discontinuity at $c_2 = 0$.

The conclusion is then that the Kisslinger-model wave function $\chi(r)$ and its logarithmic derivative $\lambda(R)$ are in general not continuous functions of the interaction parameters b and c, there being in particular a discontinuity in $\lambda(R)$ as $c_2 \equiv \mathrm{Im}c$ passes through zero. Since $I_1 = \pm i\pi/g$, where $g \equiv r_0^2\alpha'(r_0) = -r_0^2\rho'(r_0)/\rho(r_0)$, this discontinuity depends inversely on the gradient of the nuclear density at the singular point. These wave-function branch-point effects will evidently be absent in only three cases:

(i) If $\alpha(0) = c_1\rho(0) > -1$, there is no singular point near physical values of r.

(ii) If $B = \Psi(r_0) = 0$ [Eqs. (A7) and (A8)] the singular component is absent from the physical solution.

(iii) In the limit of a uniform square-well nuclear-density distribution, $g \to \infty$ and $I_1 \to 0$.

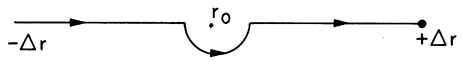

FIG. 8. z-plane contour.

APPENDIX B: SOME COMPUTATIONAL TECHNIQUES FOR THE KISSLINGER MODEL

In this appendix, we list some formulas useful in the practical problem of integrating the Kisslinger-model radial equation and adjusting the nuclear interaction parameters to make the resulting wave function satisfy assigned boundary conditions at some radius R just outside the nucleus. Local potential models are of course included as the special case where the gradient interaction function $\alpha(r)$ is identically zero. It is convenient for the following derivations to split the Kisslinger-model radial equation (A1) into a pair of coupled linear first-order differential equations:

$$\Psi(r) = r^2[1+\alpha(r)]\frac{d\chi}{dr} \quad \text{(B1a)}$$

and

$$\frac{d\Psi}{dr} = Q(r)\chi(r) , \quad \text{(B1b)}$$

where

$$Q(r) \equiv r^2[U(r) - k^2] + l(l+1)[1+\alpha(r)] \,. \qquad \text{(B1c)}$$

This form was also necessary for the numerical integration routine (Berkeley ZAM) that was available. Given l, k^2, $U(r)$, and $\alpha(r)$, this routine was set up to generate the solution with the form $\chi(r) \sim \text{const} \times r^l$ near the origin ($r=0$). The logarithmic derivative of this wave function, defined as

$$\lambda \equiv 1 + (1+\alpha)\frac{r\chi'}{\chi}\bigg|_{r=R} = 1 + \Psi(R)/R\chi(R) \,, \qquad \text{(B2)}$$

depends implicitly on the choice of $U(r)$ and $\alpha(r)$. To investigate the changes in λ due to changes in (U, α), we compare the solution (χ, Ψ) of Eq. (B1) with the solution $(\hat{\chi}, \hat{\Psi})$ generated by an alternate choice $(\hat{U}, \hat{\alpha})$:

$$\hat{\Psi} = r^2(1+\hat{\alpha})\hat{\chi}' \,, \quad \hat{\Psi}' = \hat{Q}\hat{\chi} \,, \quad \text{etc.} \qquad \text{(B3)}$$

By usual multiplication of Eq. (B1b) by $\hat{\chi}$, Eq. (B3) by χ, and subtraction we have

$$\hat{\chi}\Psi' - \chi\hat{\Psi}' = (Q - \hat{Q})\hat{\chi}\chi \,. \qquad \text{(B4a)}$$

Use of Eqs. (B1a) and (B3) allows this to be rewritten as

$$\frac{d}{dr}(\hat{\chi}\Psi - \chi\hat{\Psi}) = (Q - \hat{Q})\hat{\chi}\chi + r^2(\alpha - \hat{\alpha})\hat{\chi}'\chi' \,. \qquad \text{(B4b)}$$

Integration from 0 to R, and division by $R\hat{\chi}(R)\chi(R)$ then results in an exact formula for the logarithmic derivative shift due to the change $(U, \alpha) \to (\hat{U}, \hat{\alpha})$:

$$\lambda - \hat{\lambda} = [I_U(R) + I_\alpha(R)]/R\hat{\chi}(R)\chi(R) \,, \qquad \text{(B5a)}$$

where

$$I_U(R) \equiv \int_0^R [U(r) - \hat{U}(r)]r^2\hat{\chi}(r)\chi(r)dr \qquad \text{(B5b)}$$

and

$$I_\alpha(R) \equiv \int_0^R [\alpha(r) - \hat{\alpha}(r)] \times [l(l+1)\hat{\chi}(r)\chi(r) + r^2\hat{\chi}'(r)\chi'(r)]dr \,. \qquad \text{(B5c)}$$

This general formula has several interesting special cases:

(i) If

$$\hat{\alpha}(r) = \alpha(r) \,,$$
$$\hat{U}(r) = U_N(r) + t'2\eta k v(r) \,,$$

and

$$U(r) = U_N(r) + t2\eta k v(r) \,,$$

then Eqs. (B5) reduce to Eq. (23) of the text, leading directly for this model to the formula (28) for the Coulomb difference D_l.

(ii) With the same (U, α), but $\hat{\alpha} = \hat{U} = 0$, the comparison solution is just the spherical Bessel function: $\hat{\chi}(r) = j_l(kr)$. Then, after a partial integration on I_α [utilizing Eq. (B3) and assuming $\alpha(R) = 0$], Eqs. (B5) yield an integral representation for the neutral ($t=0$) logarithmic derivative in terms of the normalized internal wave function $y(r) = r\chi(r)/R\chi(R)$:

$$\lambda = 1 + \frac{kRj_l'(kR)}{j_l(kR)} + \int_0^R dr\, y(r) \times \left[\frac{rj_l(kr)[U_N(r) + k^2\alpha(r)] - krj_l'(kr)\alpha'(r)}{j_l(kR)}\right] . \qquad \text{(B6)}$$

Of course if $\chi(r)$ were known, λ would be given by Eq. (B2). But conversely if λ were the known quantity (e.g., Table II), $y(r)$ would be strongly constrained [cf. Eq. (27) of text] and Eq. (B6) could be used to display the contribution to λ of the various terms in the wave equation. Similar formulas for the other charges ($t = \pm 1$) may be derived using $\hat{U}(r) = 2\eta kt/r$. Then $(kr)j_l(kr)$ is replaced by the regular Coulomb function $F_l(t\eta; kr)$, and Eq. (B6) has an additional Coulomb term.

(iii) Suppose U and α depend on a set of parameters $s = (s_1, s_2, \ldots, s_n)$: $U = U(s; r)$ and $\alpha = \alpha(s; r)$. Then the logarithmic derivative $\lambda(s)$ will also depend on these parameters, and Eq. (B5) may be used to construct the derivatives $\partial\lambda/\partial s_i$ from a single calculation of the wave function $\chi(s; r)$. This permits the use of efficient gradient-type iteration methods to adjust the parameters to match an assigned value of λ. Taking $\hat{U} = U(\hat{s}; r)$ and $\hat{\alpha} = \alpha(\hat{s}; r)$, where $\hat{s} = (s_1, s_2, \ldots, s_i + \Delta s_i, \ldots, s_n)$, in the limit $\Delta s_i \to 0$ we have

$$\hat{\chi} = \chi(\hat{s}; r) \to \chi(s; r)$$

and

$$\frac{\partial\lambda}{\partial s_i} = \frac{1}{R\chi(R)^2}\int_0^R dr\left([r\chi(r)]^2\frac{\partial U}{\partial s_i} + \{l(l+1)\chi(r)^2 + [r\chi'(r)]^2\}\frac{\partial\alpha}{\partial s_i}\right) . \qquad \text{(B7)}$$

In Sec. IV we used $U(r) = (b_1 + ib_2)\rho(r)$ and $\alpha(r) = (c_1 + ic_2)\rho(r)$. The parameter set is $s = (b_1, b_2, c_1, c_2)$, and Eq. (B7) was used with $\partial U/\partial b_1 = \rho(r)$, etc., to fit the calculated λ's to the empirical ones. Note that if U and α are analytic functions of a complex variable $z = s_1 + is_2$, and so satisfy the Cauchy-Riemann conditions ($\partial U/\partial s_2 = i\partial U/\partial s_1$, etc.), then $\lambda(z)$ is also analytic in z be-

cause it also satisfies these conditions. The one restriction to be observed is that if the parameters are such that $\chi(s;r)$ has a branch cut (cf. Appendix A), $\hat{s}$ and s must be chosen on the same side of the cut to achieve $\hat{\chi} \to \chi$ in the limit $\hat{s} \to s$. In this connection, note that substituting the complex conjugates of U and α into Eq. (B1) does not necessarily generate the complex conjugate of χ. Therefore use of Eq. (B5) to construct $\lambda - \lambda^* = 2i\,\mathrm{Im}\lambda$ must be done with caution. These restrictions are not necessary if $\alpha(r) > -1$ everywhere, as in the special case of local potential models where $\alpha(r) \equiv 0$.

---

*Work done under auspices of the U. S. Atomic Energy Commission under Contract No. W-7405-eng-48.

†Presently NAS-NRC Research Associate, Theoretical Studies Branch, code 641, Goddard Space Flight Center, Greenbelt, Md. 20771.

[1]M. M. Sternheim and R. Hofstadter, Nuovo Cimento 38, 1854 (1965).

[2]E. H. Auerbach, D. M. Fleming, and M. M. Sternheim, Phys. Rev. 162, 1683 (1967); 171, 1781 (1968).

[3]K. M. Crowe, A. Fainberg, J. Miller, and A. S. L. Parsons, Phys. Rev. 180, 1349 (1969).

[4]M. Ericson, Nuovo Cimento 47, 49 (1967).

[5]L. I. Schiff, Progr. Theoret. Phys. (Kyoto) Suppl. Extra No., 400 (1965).

[6]M. E. Nordberg, Jr., and K. F. Kinsey, Phys. Letters 20, 692 (1966).

[7]J. P. Antoine, Nuovo Cimento 44A, 1068 (1966).

[8]G. B. West, J. Math. Phys. 8, 942 (1967); Phys. Rev. 162, 1677 (1967).

[9]M. M. Block, Phys. Letters 25B, 604 (1967).

[10]P. R. Auvil, Phys. Rev. 168, 1568 (1968).

[11]M. M. Block, I. Kenyon, J. Keren, D. Koetke, P. Malhotra, and H. Winzeler, Phys. Rev. 169, 1074 (1968).

[12]S. Rae and P. Thurnauer, Phys. Rev. 180, 1387 (1969).

[13]R. A. Christensen, Phys. Rev. D 1, 1469 (1970).

[14]G. C. Oades and G. Rashe, Nucl. Phys. B20, 333 (1970); G. C. Oades *et al.*, Nuovo Cimento 2A, 438 (1971).

[15]H. Frank, D. Haas, and H. Prange, Phys. Letters 19, 391 (1965); 19, 719 (1965); G. R. Burleson and H. W. Kendall, Nucl. Phys. 19, 68 (1960).

[16]The error function is defined by

$$\mathrm{erf}(z) \equiv \frac{2}{\sqrt{\pi}} \int_0^z e^{-x^2} dx \equiv 1 - \mathrm{erfc}(z).$$

[17]Equation (15) was derived using Bateman manuscript Project, *Tables of Integral Transforms,* edited by A. Erdelyi (McGraw-Hill, New York, 1954), Vol. 1, p. 74, formula 26. We take $a = a_N$.

[18]Geoffrey F. Chew, *S-Matrix Theory of Strong Interactions* (Benjamin, New York, 1961), Chap. 15; Richard Wilson, Phys. Today 22, No. 1, 47 (1969); S. D. Drell and F. Zachariasen, *Electromagnetic Structure of Nucleons* (Oxford Univ. Press, Oxford, England, 1961).

[19]K. M. Watson, Phys. Rev. 105, 1388 (1957); A. L. Fetter and K. M. Watson, *Advances in Theoretical Physics,* edited by K. A. Brueckner (Academic, New York, 1965), p. 115.

[20]M. Ericson and T. E. O. Ericson, Ann. Phys. (N.Y.) 36, 323 (1966).

[21]L. S. Kisslinger, Phys. Rev. 98, 761 (1955).

[22]J. V. Lepore and R. J. Riddell (private communication).

[23]See Table VI of Ref. 3.

[24]J. Rix and R. M. Thaler, Phys. Rev. 152, 1357 (1966).

[25]I would like to thank Dr. Alfred Goldhaber for this suggestion.

[26]E. T. Whittaker and G. N. Watson, *A Course of Modern Analysis* (Cambridge Univ. Press, Cambridge, England, 1962), Chap. X.